Chemistry–A European Journal
Research Article
doi.org/10.1002/chem.202303701
Chemistry Europe
European Chemical Societies Publishing
www.chemeurj.org

Polar covalent apex-base bonding in borapyramidanes probed by solid-state NMR and DFT calculations

Dominique J. Luder,[a, b] Nicole Terefenko,[a] Qiu Sun,[c] Hellmut Eckert,[d, e] Christian Mück-Lichtenfeld,[c] Gerald Kehr,[c] Gerhard Erker,*[c] and Thomas Wiegand*[a, f]

Pyramidane molecules have attracted chemists for many decades due to their regular shape, high symmetry and their correspondence in the macroscopic world. Recently, experimental access to a number of examples has been reported, in particular the rarely reported square pyramidal bora[4]pyramidanes. To describe the bonding situation of the nonclassical structure of pyramidanes, we present solid-state Nuclear Magnetic Resonance (NMR) as a versatile tool for deciphering such bonding properties for three now accessible bora[4]pyramidane and dibora[5]pyramidane molecules. ^{11}B solid-state NMR spectra indicate that the apical boron nuclei in these compounds are strongly shielded (around −50 ppm vs. BF_3-Et_2O complex) and possess quadrupolar coupling constants of less than 0.9 MHz pointing to a rather high local symmetry. ^{13}C–^{11}B spin-spin coupling constants have been explored as a measure of the bond covalency in the borapyramidanes. While the carbon-boron bond to the $-B(C_6F_5)_2$ substituents of the base serves as an example for a classical covalent 2-center-2-electron (2c–2e) sp^2-carbon-sp^2-boron σ-bond with $^1J(^{13}C\text{-}^{11}B)$ coupling constants in the order of 75 Hz, those of the boron(apical)-carbon(basal) bonds in the pyramid are too small to measure. These results suggest that these bonds have a strongly ionic character, which is also supported by quantum-chemical calculations.

Introduction

Given their regular shape and high symmetry, the [4]pyramidane C_5H_4, composed of a C_4 base and an apical carbon atom on top of that base, evoked the interest of chemists more than four decades ago.[1] In [n]pyramidanes (n denotes the number of atoms in the base), the apically positioned atom is forced into an unusual geometry, resulting in interatomic apex-to-pyramid base interactions not described by classical bond theory.[2] While first studies of pyramidanes were limited to *in-silico* investigations, the synthesis was reported for a variety of pyramidanes in recent years (for comprehensive review articles see references).[3] This includes, among others, the lithium and magnesium cyclobutadiene salts, as well as bora-, sila- and stannapyramidanes.[4] A synthetic approach on the reversible conversion from a classical borole to the nonclassical isomer, the bora[4]pyramidane, by photolysis was recently reported.[4e]

The non-classical bonding interactions of the apical atom to the pyramid base are of central interest in the studies of pyramidanes. For the systems investigated so far, a broad range of bonding interactions has been proposed, from purely ionic to covalent, depending on the apical group, as well as on the substitution pattern at this group or at the pyramid base. One example for the limiting case of covalent interactions is the hypothetical C_5H_4 [4]pyramidane (which has never been synthesized, but has been subject to theoretical investigations[1a,2a,4g,5]), while purely ionic examples comprise the lithium and magnesium cyclobutadiene salts (see Scheme 1a, A=$[Li^+]_2$, respectively A=$[Mg^{2+}]$).[4c,d] Placed in-between, with bonding interactions denoted as "polar covalent", are group-14 [4]pyramidanes featuring Ge, Sn or Pb as the apical atom (see Scheme 1b, A=Ge, Sn, Pb) or the group-13 bora[4]pyramidane (see Scheme 1b, A=BCl).[4f,6] Very recently, also stable sila[4]pyramidanes have been reported.[4a] A combination of analytical and computational techniques was applied to study the bonding properties of pyramidanes, including X-ray crystallography, Mößbauer spectroscopy,[4b] solution-state NMR spectroscopy and optical spectroscopies, such as UV-Vis absorption and Raman scattering.[6] Computational methods include among others natural resonance theory (NRT), the

[a] D. J. Luder, N. Terefenko, Prof. Dr. T. Wiegand
Institute of Technical and Macromolecular Chemistry, RWTH Aachen University, Worringerweg 2, 52074 Aachen (Germany)
[b] D. J. Luder
Laboratory of Physical Chemistry, ETH Zürich, Vladimir-Prelog-Weg 2, 8093 Zürich (Switzerland)
[c] Dr. Q. Sun, Dr. C. Mück-Lichtenfeld, Dr. G. Kehr, Prof. Dr. G. Erker
Organische Chemie, University of Münster, Corrensstr. 36, 48149 Münster (Germany)
E-mail: erker@wwu.de
[d] Prof. Dr. H. Eckert
Instituto de Física de São Carlos, Universidade de São Paulo, São Carlos, SP 13566–590 (Brazil)
[e] Prof. Dr. H. Eckert
Institut für Physikalische Chemie, University of Münster, Corrensstr. 30, 48149 Münster (Germany)
[f] Prof. Dr. T. Wiegand
Max Planck Institute for Chemical Energy Conversion, Stiftstr. 34–36, 45470 Mülheim (Germany)
E-mail: thomas.wiegand@cec.mpg.de

Supporting information for this article is available on the WWW under https://doi.org/10.1002/chem.202303701

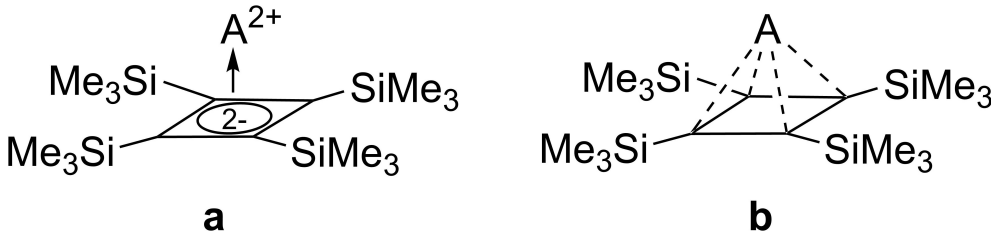

Scheme 1. Schematic representation of limiting cases of bonding scenarios in [4]pyramidane-type molecules: Ionic (**a**) and covalent (**b**) description. Dashed lines in **b** represent 5c–6e (apex-base) bonds.

topological analysis method Atoms in Molecules (AIM) and nucleus-independent chemical shift (NICS) calculations.[4b–d,f,6–7]

We studied three representative borapyramidane molecules and compared them to a borole as the reference molecule by solid-state NMR and quantum-chemical investigations to unravel their solid-state bonding properties. The selected compounds for our study originate from a reaction sequence (see Scheme 2), in which the borole **1** was converted to its structural isomer [4]pyramidane **2** upon exposure to light. When **2** was heated in the presence of SMe_2, the borole **1** was reformed, while irradiation at elevated temperature led to the rearrangement of **2** into the more symmetric isomeric [4]pyramidane **3**.[4e] The [4]pyramidane **3** reacted with $HB(C_6F_5)_2$ under framework extension to the [5]pyramidane **4** (the synthesis of compound **4** will be described in detail by Q. Sun et al. in a forthcoming publication, for a short description see Supplementary Information).[8]

Among the experimental analytical techniques used to study pyramidanes, detailed solid-state NMR spectroscopic studies have been scarce, despite their high potential for probing bonding properties in the solid state, as for instance demonstrated in studying the bonding interactions in phosphane-borane frustrated Lewis pairs (FLPs) and related compounds (for selected reviews see[9]). In the case of the pyramidane apical atom containing a quadrupolar nucleus (nuclear spin quantum number $I > 1/2$, examples are $^{6/7}$Li, $^{10/11}$B, ^{25}Mg and ^{73}Ge), the NMR line shape recorded under magic-angle spinning (MAS) conditions directly reports on the local electric-field gradient (EFG) at the quadrupolar nucleus (whose lineshape modification can be described by first- or second-order perturbation theory), which is highly sensitive to the symmetry of the surrounding electron density distribution. A higher symmetry at the nuclear site leads to a smaller EFG and thus a smaller quadrupolar coupling constant. Contrary to NMR measurements in the solution state,[10] the quadrupolar relaxa-

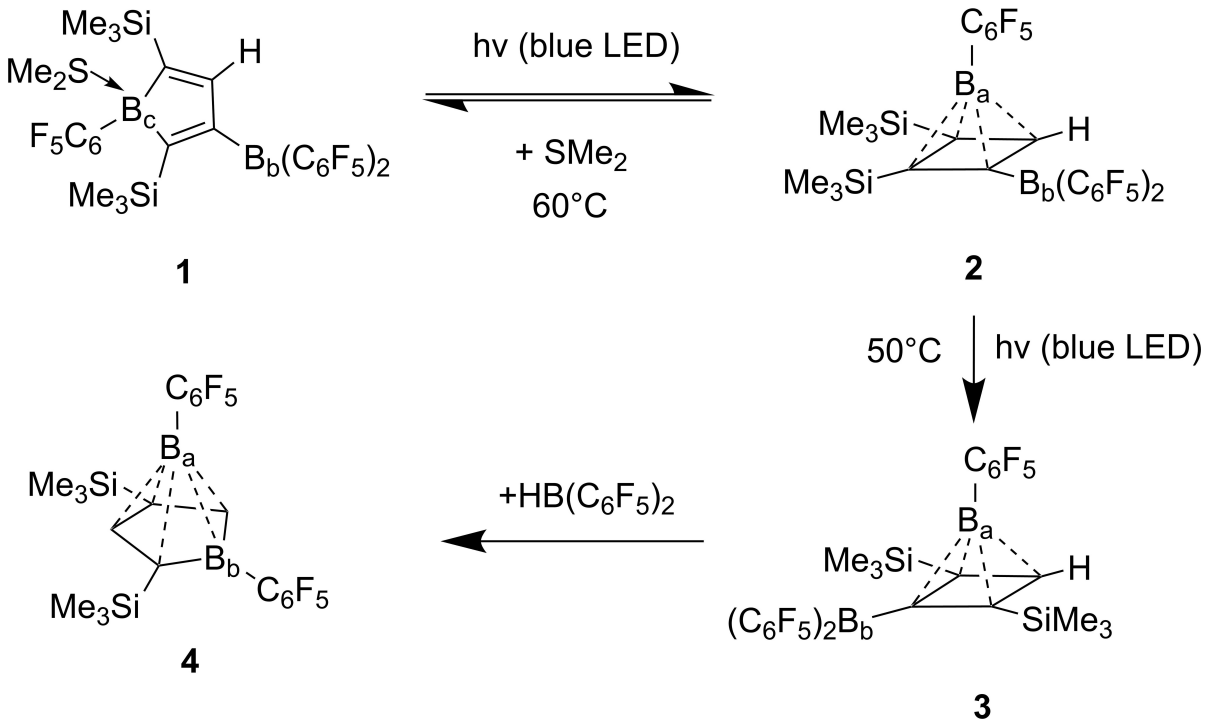

Scheme 2. Reaction sequence for the investigated compounds: **1** borole, **2** and **3** bora[4]pyramidanes and **4** dibora[5]pyramidane molecules. nc-6e bonds are shown as dashed lines. Boron atoms in **2**–**4** are labelled according to their apical (B_a) or basal (B_b) position with respect to the pyramidal shape of the borapyramidanes.

tion is typically slower in the solid state owing to the absence of molecular reorientation processes.[11]

The slowed quadrupolar relaxation properties allow for probing indirect spin-spin-couplings (*J-couplings*) between the ^{13}C spin-1/2 nucleus and the ^{11}B quadrupolar nucleus ($I=3/2$) in the solid state, as for instance already reported for ^{69,71}Ga-^{31}P (ref.[12]), ^{55}Mn-^{31}P (ref.[13]), ^{99,101}Ru-^{31}P (ref.[14]), ^{63,65}Cu-^{31}P (ref.[15]), ^{95,97}Mo-^{31}P (ref.[16]) and ^{11}B-^{31}P (ref.[17]) spin pairs. *J*-couplings in the NMR spectra directly point to the presence of covalent bonding character (since nuclear spin polarization is transferred to other nuclei by spin-polarization of σ-bonding electrons). Therefore, they can be used to describe the bonding situation, for instance between the apical atom and the pyramid base carbon atoms.[18] Note, that indirect spin-spin couplings have also been reported in the solid state across hydrogen bonds,[19] as well as upon interaction of nonbonded electrons ("through-space" interaction, see for instance reference[20]).

Another key NMR observable in describing the bonding properties of borapyramidanes is the isotropic ^{11}B chemical shift of the apical boron nucleus: In solution, the resonance appears at unusually low frequencies near $\delta=-50$ ppm in dibora[5]pyramidane **4**.[8] In the solid state, similarly shielded boron sites have been observed for instance in borohydrides and a borocenium cation, with the latter being formally described as a bora[5]pyramidane.[21]

Our solid-state NMR investigations are supplemented with density functional theory (DFT) calculations of chemical-shift values and indirect spin-spin coupling constants. Calculations of the ^{11}B EFG tensors by DFT allowed comparison of theoretical and experimental quadrupolar coupling constants (C_Q) and electric field gradient asymmetry parameters (η_Q), as well as visualization of the individual tensor components in the molecular-axis frame.[22] To identify whether delocalization of electrons in the pyramidal plane, leading to ring current effects, is present (reminiscent to the Hückel aromatic 6π electron-containing dianionic cyclobutadiene salts), NICS calculations have often been used as a criterion for aromaticity.[23] Additionally, bond topology analysis was performed employing the AIM method[24] as well as Natural Bond Order (NBO) analysis[25] to describe the nature of the pyramid apex-to-base interatomic interactions.

Results and Discussion

The apical boron nuclei in the borapyramidanesare strongly shielded and possess a small ^{11}B quadrupolar coupling constant

The borole and borapyramidanes shown in Scheme 2 were characterized by ^{11}B solid-state NMR MAS spectroscopy to probe the local electron distribution at the boron nuclei. The ^{11}B MAS spectra of **1** and **2** are given in Figure S1, the ones of **3** and **4** are shown in Figure 1, top panel. Simulation of the ^{11}B MAS quadrupolar line shape of the three-coordinated boron nucleus of the $-B(C_6F_5)_2$ substituent, denoted as B_b in the following (see Scheme 2), allowed determining experimental C_Q- and η_Q-values (see Table 1 and Table S1). Since the ^{11}B MAS spectra only allow for unambiguous line-shape simulation of the B_b site with the larger C_Q, ^{11}B satellite transition spectroscopy (SATRAS[26]) experiments were applied for determining the C_Q-values of the apical boron atom, denoted as B_a in the following, see Figure 1, bottom panel and Table 1. For all the SATRAS spectra see Figure S2. In the latter, the simulation of the MAS sideband profile arising from the non-central $m=1/2 \leftrightarrow m=3/2$ Zeeman transitions enables an accurate determination of small C_Q-values.

The ^{11}B resonances of **1** serve as a reference in our study and are detected at chemical-shift values of 0.2 and 61.7 ppm (B_c and B_b in Scheme 2, respectively), which is within the typical chemical-shift range expected for classical four- and three-coordinated boron atoms, respectively.[27] The coordination state is further encoded in the C_Q-values, with a rather large value (4.4 MHz) detected for the three-coordinated B_b, and a smaller value (1.9 MHz) for the four-coordinated B_c site (see Table 1). The smaller C_Q-value directly reports on a smaller EFG and thus a higher local symmetry as expected for B_c (or vice versa for B_b). Similar η_Q-values of 0.2 are found for both boron species pointing to rather small deviations from axial symmetry.

The boron atoms B_b of bora[4]pyramidanes **2** and **3** display ^{11}B chemical-shift values (52.8 ppm and 58.5 ppm for B_b(**2**) and B_b(**3**), respectively), C_Q-values (4.0 MHz and 4.1 MHz for B_b(**2**) and B_b(**3**), respectively) and $_{\eta Q}$-values (0.2 for both, B_b(**2**) and B_b(**3**)) typical for close-to-trigonally-coordinated boron atoms, comparable to the observed values for B_b in the borole **1**.[27–28] In contrast, both chemical-shift and quadrupolar interaction parameters are strikingly different for the pyramidal apical boron atom B_a. In **3**, a ^{11}B chemical shift of $\delta(B_a)$ −47.3 ppm is observed, with $C_Q=0.7$ MHz and $\eta_Q=0.4$ indicating a higher symmetry of the electron distribution (a smaller ^{11}B EFG represented by the small value for C_Q) compared to the B_b site and a slight increase in the asymmetry parameter η_Q. For **2**, a similar ^{11}B chemical-shift value, but a slightly larger C_Q-value of 0.9 MHz and an increased η_Q-value of 0.7 was found, possibly

Table 1. ^{11}B isotropic chemical shift δ_{iso}, quadrupolar coupling constant C_Q and asymmetry parameter η_Q for the investigated compounds.

	δ_{iso} (exp., ppm)[b]	C_Q (exp., MHz)	η_Q (exp.)	δ_{iso} (calc., ppm)	$\lvert C_Q \rvert$ (calc., MHz)	η_Q (calc.)
1, B_c	0.2	1.9[c]	0.2[c]	−2.4	2.0	0.1
1, B_b	61.7	4.4[b]	0.2[b]	58.7	4.3	0.2
2, B_a	−47.6	0.9[c]	0.7[c]	−50.9	0.9	0.7
2, B_b	52.8	4.0[b]	0.2[b]	51.0	3.9	0.2
3, B_a	−47.3	0.7[c]	0.4[c]	−51.9	0.7	0.4
3, B_b	58.5	4.1[b]	0.2[b]	56.2	4.1	0.2
4, B_a	−50.2	0.7[c]	0.2[c]	−55.3	0.7	0.3
4, B_b	20.0	2.4[b]	0.1[b]	19.0	2.4	0.1

[a] Chemical shifts δ_{iso} were calculated on a DFT B3-LYP/def2-TZVP, electric field gradient on a DFT B97-D/def2-TZVP (modified) level of theory. [b] Determined from line-shape analysis of ^{11}B MAS EASY spectra. [c] Determined from line shape analysis of ^{11}B SATRAS spectra.

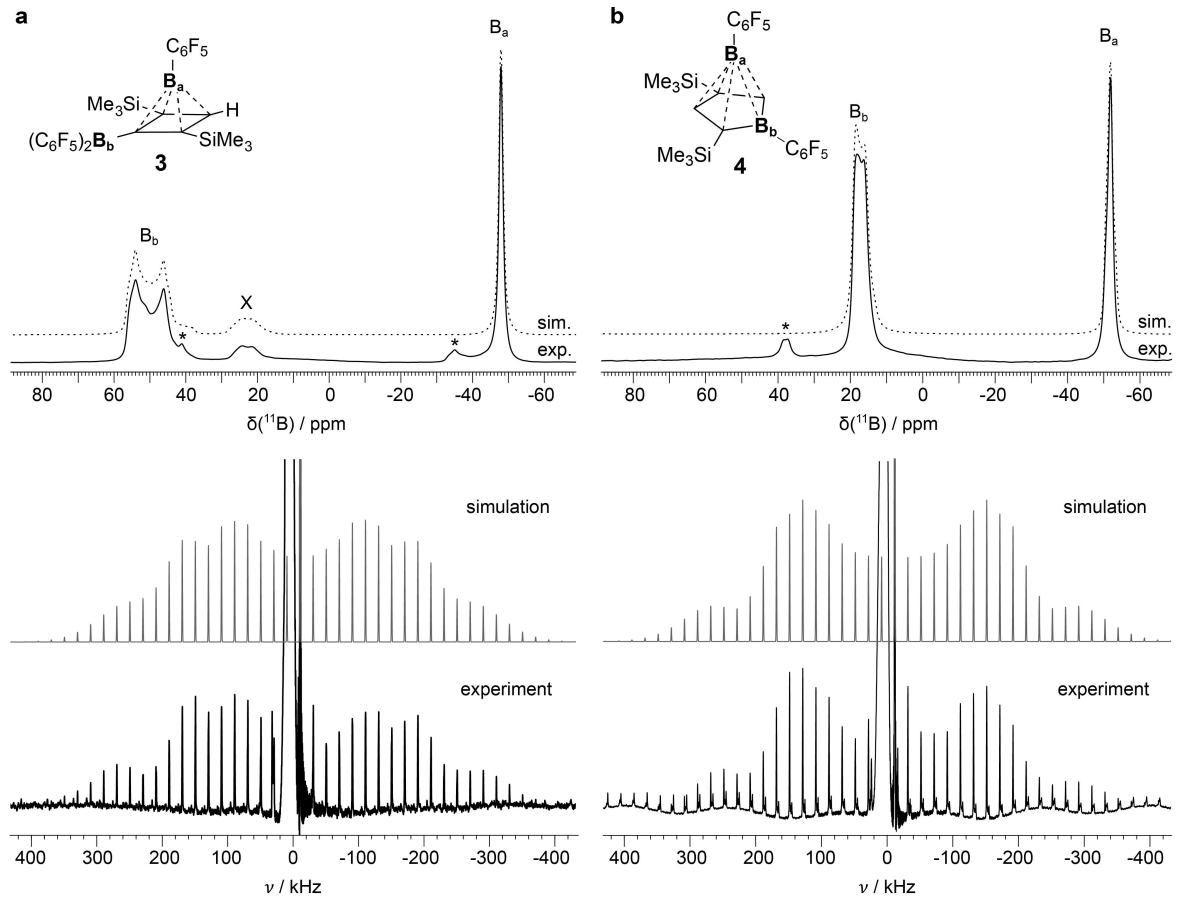

Figure 1. *The apical boron nucleus in bora[4]- and dibora[5]pyramidanes resonates at unusually low frequencies and possesses a small quadrupolar coupling constant.* (a) ^{11}B MAS and SATRAS spectra including line-shape simulation of bora[4]pyramidane **3**. (b) ^{11}B MAS and SATRAS spectra including line-shape simulation of dibora[5]pyramidane **4**. In the top spectra, resonances marked with * correspond to MAS side bands and resonance x originates from a hydrolysed species. In the SATRAS spectra at the bottom, the MAS sideband manifolds belonging to the $m = \pm 1/2 \leftrightarrow m = \pm 3/2$ ("satellite" transitions) are observed for the boron resonance pertaining to B_a. All spectra were recorded at 16.4 T employing a MAS frequency of 20 kHz.

originating from the different coordination of the C_4-base in **2** and **3** (*vide infra*). Similar strongly shielded apical nuclei have been commonly observed for pyramidanes in solution-state NMR spectra,[4a,c, g] as well as for a borocenium cation in the solid state.[21b] In contrast, less negative ^{11}B isotropic chemical-shift values were reported for carboranes (icosahedral carborane $C_2B_{10}H_{12}$ nuclei for instance resonate between −1 to −17 ppm).[29] Accompanying the solid-state NMR measurements, we performed magnetic-shielding and EFG tensor calculations in the gas phase, which in most cases is sufficient to accurately calculate NMR observables. The obtained DFT-calculated quadrupolar parameters, C_Q and η_Q, are indeed in good agreement with experimentally-determined values (see Table 1).[22b]

The principal components of the calculated EFG tensor can be visualized within the molecular structures (see Figure 2). The main component, V_{zz}, of the EFG tensor (which is the largest component of the EFG tensor and directly proportional to the measured C_Q-value) for the bora[4]pyramidanes **2** and **3** point towards the pyramid base (see Figure 2), although not directly to the centre of mass of the C_4-base due to the absence of overall C_{4v} symmetry, which is also reflected in deviations of the η_Q-value from zero (axial symmetry). Comparable findings were made in a previous ^{11}B MAS solid-state NMR study on a borocenium cation, in which the V_{zz} component of the apical ^{11}B EFG tensor points towards the Cp* base.[21b] While in **3** V_{zz} points in the direction of the basal CH bond, it is slightly displaced from that orientation in **2** towards one of the $SiMe_3$ substituents.

In **4**, the B_b site (now the B_b boron nucleus is part of the pyramid base) reveals a smaller C_Q-value (2.4 MHz) compared to the $-B(C_6F_5)_2$ substituents in **1**, **2** and **3** indicating a profound change in the trigonal coordination state, although the bond angle sum is still close to 360° deduced from the crystal structure (359.1°, see Table S1c). This clearly indicates an interaction with the apical boron site (B_a) in **4**, which is absent for the $-B(C_6F_5)_2$ substituents in **2** and **3**. The low-frequency shifted ^{11}B resonance (20.0 ppm) further supports electronic interactions with the apical boron atom. This is further supplemented with the ^{11}B chemical-shift value of a five-membered C_4B borole dianion ring in solution, which has been reported at a higher chemical-shift value (36.3 ppm)[4f] and the determined value of 75.7 ppm for the SMe_2 free borole 1.[4e]

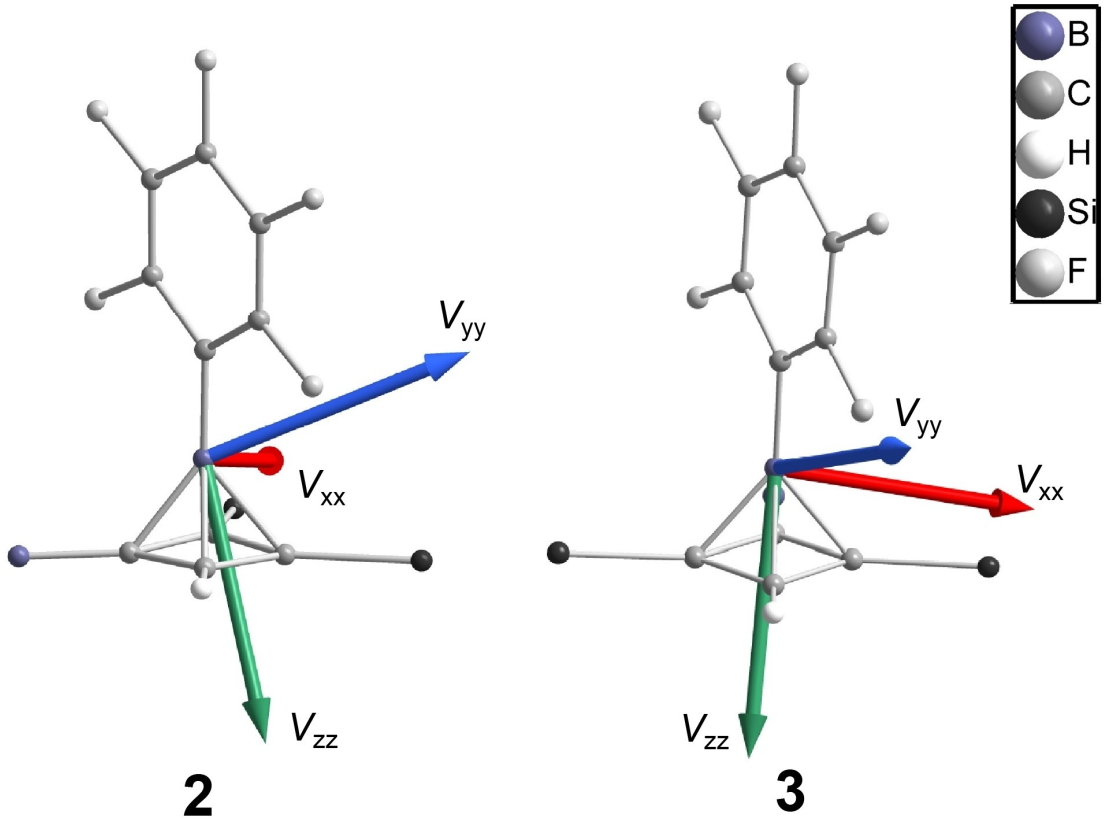

Figure 2. *The V_{zz} component of the ^{11}B EFG points towards the C_4-base.* EFG tensor orientations of bora[4]pyramidanes **2** and **3**. The EFG tensors were calculated using DFT (B97-D, def2-TZVP (modified)). For clarity, only the first atoms of the substituents to the pyramid base are shown.

^{29}Si MAS reveals the crystallographic inequivalence of the $SiMe_3$ groups in 3

The trimethylsilyl (TMS) groups are of importance in stabilizing the borapyramidane molecules due to their electron-donating character (*vide infra*).[30] Contrary to the situation in the solution state, where the two TMS groups of **3** are magnetically equivalent, the C_s-symmetry is partially broken in the crystalline form of the compound (see also the crystal structure of **3** reported in reference [4e]). ^{29}Si MAS solid-state NMR proved to be a sensitive tool for probing these changes in symmetry in the solid state and it was possible to distinguish the two TMS groups spectroscopically by their different ^{29}Si chemical-shift values (see Figure 3a for dibora[5]pyramidane **4** and bora[4]pyramidane **3**). The spectra for **1** and **2** are given in Figure S3, the deviations in the signal integrals from the expected 1 : 1 ratio in compounds **2** and **4** are subject to further investigations. An unambiguous assignment of the two ^{29}Si resonances was achieved with 2D ^{1}H-^{29}Si heteronuclear correlation (HETCOR) spectra (see Figure 3b and S4). The ^{29}Si NMR signal at −2.9 ppm, which is correlated with both ring protons must be assigned to the $SiMe_3$ group bonded to C4, whereas the signal at −4.0 ppm must be assigned to the $SiMe_3$ group bonded to C2.

Covalent bonding character assessed by ^{13}C-^{11}B spin-spin coupling constants

Figures 4 and S5 show the ^{1}H-^{13}C cross-polarization (CP) MAS NMR spectra, from which the ^{13}C—^{11}B indirect spin-spin coupling constants were determined to characterize the carbon-boron bond covalencies. Note, that such information is usually not available from solution-state spectra due to fast quadrupolar relaxation, except for cases of highly symmetric tetrahedral species.[10,31] For the studied borapyramidanes however, these *J*-couplings remain unresolved in solution-state NMR spectra.[4e] The observed line shapes observed in the solid state not only originate from ^{13}C-^{11}B pairs (^{11}B, $I = 3/2$, 80.4 %), but also from the ^{13}C—^{10}B isotopologues (^{10}B, $I = 3$, 19.6 %). In Figure 4, bottom panel, the experimental line shape is described by a line-shape simulation taking both, ^{13}C—^{11}B and ^{13}C—^{10}B *J*-couplings, into account. For a spin-1/2 nucleus interacting with a spin-3/2 species, a symmetric quartet with a 1 : 1 : 1 : 1 intensity ratio is expected. However, if the spin-3/2 nucleus experiences a significant nuclear electric quadrupolar interaction, the heteronuclear dipolar coupling is not fully averaged under MAS conditions, and hence, a residual dipolar coupling *d* results in a broadening and intensity asymmetry of the *J*-multiplets (see Figure 4, bottom panel), as also observed in the present study.[18,32] This has also been observed for example with arylboronic acids.[33]

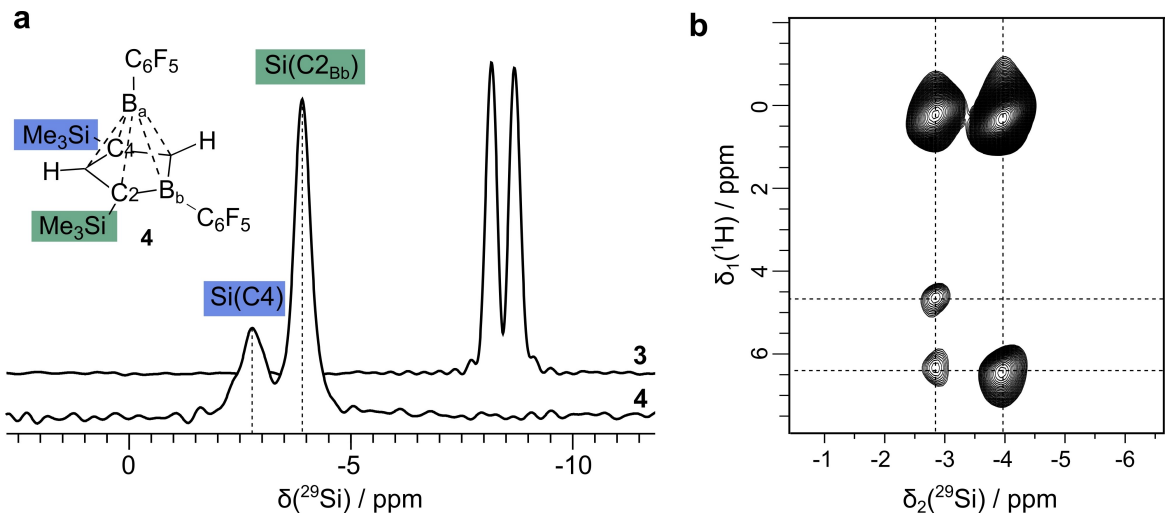

Figure 3. *^{29}Si MAS indicates reduced symmetry in the solid state.* (a) ^{29}Si MAS solid-state NMR spectrum of bora[4]pyramidane **3** and dibora[5]pyramidane **4** recorded at 16.4 T and 17 kHz MAS. (b) ^{1}H-^{29}Si HETCOR spectrum of dibora[5]pyramidane **4** recorded at 16.4 T and 17 kHz MAS. Based on the HETCOR spectrum, the ^{29}Si resonances were unambiguously assigned.

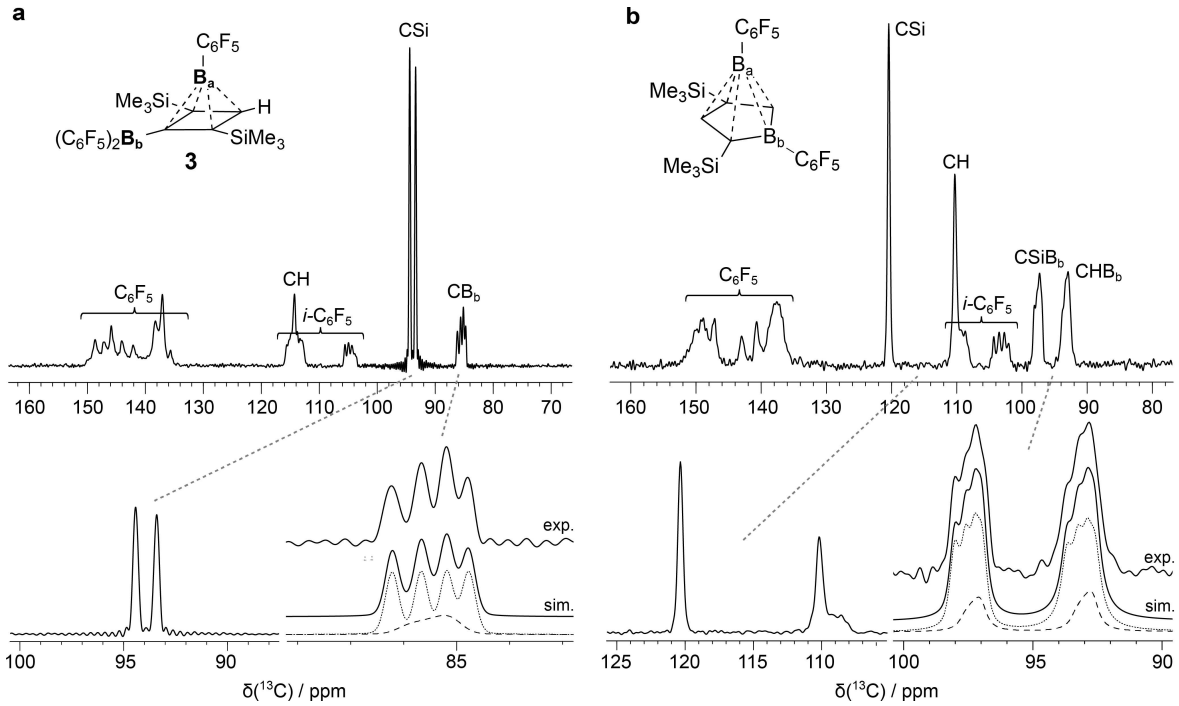

Figure 4. *^{13}C solid-state NMR spectra report on ^{13}C-^{11}B spin-spin couplings as a measure for bond covalence.* Top panel: **a** High-frequency spectral region of a ^{1}H-^{13}C CP MAS NMR spectrum of **3** recorded at 16.4 T and 17 kHz MAS, **b** High-frequency spectral region of a ^{1}H-^{13}C CP MAS NMR spectrum of **4** recorded at 11.7 T and 17 kHz. Assignment is in agreement with solution-state NMR spectroscopic data and DFT calculations (see SI,[10]). Bottom panel: horizontally expanded views focusing on selected resonances. The multiplet line shape was simulated using the DMFit[58] software. **a** ^{13}C spectrum of **3**. *J*-multiplet line-shape simulation shows the contributions arising from both, ^{13}C–^{11}B (dotted curve) and ^{13}C–^{10}B (dashed curve) spin-spin coupling. **b** ^{13}C spectrum of **4**. *J*-multiplet line-shape simulation also shows the contributions arising from ^{13}C–^{11}B (dotted curve) and ^{13}C–^{10}B (dashedcurve) spin-spin coupling.

In **2** and **3**, such peak splittings were observed for all the carbon atoms directly bonded to a boron atom via a classical 2c–2e σ-single bond. The ^{13}C MAS-NMR line shapes were simulated revealing ^{13}C–^{11}B coupling constants of $^{1}J(C_{Bb}\text{-}B_b) \approx 75$ Hz for compound **2** and $^{1}J(C_{Bb}\text{—}B_b) \approx 84$ Hz for **3**, see also Table 2 for comparison with DFT-calculated values. The coupling constant of the C_{Bb}-B_b bond thereby acts as an internal reference for a typical covalent 2c–2e carbon-boron bond. In contrast, no such peak splittings were observed for the carbon atoms at pyramid base to B_a. These singlet spectra are described by typical pseudo-Voigt functions, from which only an upper limit of $^{1}J(C_{base}\text{-}B_a) = 18$ Hz can be estimated from the observed ^{13}C NMR linewidth. Consistent with this experimental result, the corresponding $J(^{13}C_{base}\text{—}^{11}B_a)$ coupling constants

Table 2. ^{13}C-^{11}B indirect spin-spin coupling constants for the investigated compounds.

	$J(C_{Bb}–B_b)$ (exp./calc.[a], Hz)	$J(iC_6F_5–B_b)$ (exp./calc.[a], Hz)	$J(C_{Bb}–B_a)$ (calc.[a], Hz)	$J(C_{Si}–B_a)$ (exp./calc.[a], Hz)	$J(C_H–B_a)$ (exp./calc.[a], Hz)	$J(iC_6F_5–B_a)$ (exp./calc.[a], Hz)
2[b]	75/93.4	49, 52/67.9, 71.9	3.3[c]	<18, 20/7.7, −2.3	<35/1.3	85/118.0
3[b]	84/94.7	–[d]/69.7, 69.4	6.4[c]	<13, 13/1.8, 0.7	<16/−1.4	98/118.1
4[e]	46, 45/56.9, 56.3	87/82.5	−1.2, −4.3[c]	<13/−3.7	<16/0.5	94/107.4

[a] The calculated isotropic coupling constants, ^1J (calc.), resulting from DFT calculations (B3-LYP/TZVP). [b] Experimental values determined from line-shape analysis of ^{13}C CP MAS spectra recorded at 16.4 T. [c] No experimental value can be determined as the line-shape is dominated by the B_b-C_{Bb} J-coupling. [d] No experimental value can be determined as two resonances overlap in the spectrum. [e] Experimental values determined from line-shape analysis of ^{13}C CP MAS spectra recorded at 11.7 T.

calculated for **2**–**4** do not exceed 7 Hz. These findings suggest a bonding interaction between the pyramid base and B_a that is fundamentally different to the classical covalent reference carbon-boron 2c–2e σ-bond. The calculated *J*-coupling constant is negative for certain B_a-pyramid-base bonds and the values are consistently dominated by the Fermi-contact contribution (see Tables S3).

In dibora[5]pyramidane **4**, we also observe a smaller indirect ^{13}C-^{11}B spin-spin coupling constant of ~45 Hz between B_b and the bound carbon atoms that are part of the pyramid base (C2 and C5) when compared to the C–B 2c–2e bonds in **2** and **3** (see Figure 4b, bottom panel and Table 2), whereas the ^1J-(^{13}C-^{11}B) value measured and calculated for B-*i*C_6F_5 is similar to those involving the basal B atoms in the bora[4]pyramidanes. The smaller isotropic coupling constants with the 5-membered base of **4** might indicate a lower degree of covalency compared to classical C–B 2c–2e bonds. For a nido-2,3,4,5-tetracarbahexaborane a $^1J(C_{base}–B_b)$ value of 59 Hz has been reported, one of the rare cases for which such values have been accessible in solution.[34]

Aromaticity criteria from ^{1}H chemical-shift values and NICS calculations

To examine whether the proton atoms within the C_4-plane experience ring-current effects caused by an aromatic character of the C_4-unit, we recorded ^{1}H MAS experiments at 60 kHz MAS. The proton resonances in **2, 3** and **4** are deshielded ($\delta(^1H, \mathbf{2}) =$ 5.5 ppm, $\delta(^1H, \mathbf{3}) = 5.7$ ppm and $\delta(^1H, \mathbf{4}) = 4.6$ and 6.5 ppm, see Figure 5a and Figure S6), however these values are not definitive indicators for aromaticity. Olefinic cyclobutadiene protons for instance resonate at 6.0 ppm in solution[35] and thus at values very similar to the ones detected for the bora[4]pyramidanes.

We thus performed NICS calculations (see Figure 5b). As in the aromaticity evaluation of group 14 pyramidanes with NICS in reference,[6] an extended analysis was applied[23a,e, f] allowing to differentiate π ring currents from σ bonding effects.[23d,e] The obtained NICS(0) values of −14.0 ppm (**3**) and −16.9 ppm (**4**) indicate aromaticity. An analysis in terms of in-plane ($\sigma_{xx} + \sigma_{yy}$) and out-of-plane ($\sigma_{zz}$) components is shown in Figure 5b for the bora[4]pyramidane **3** (see SI for analysis of **2** and **4**). The trajectory of the NICS curves of all investigated compounds

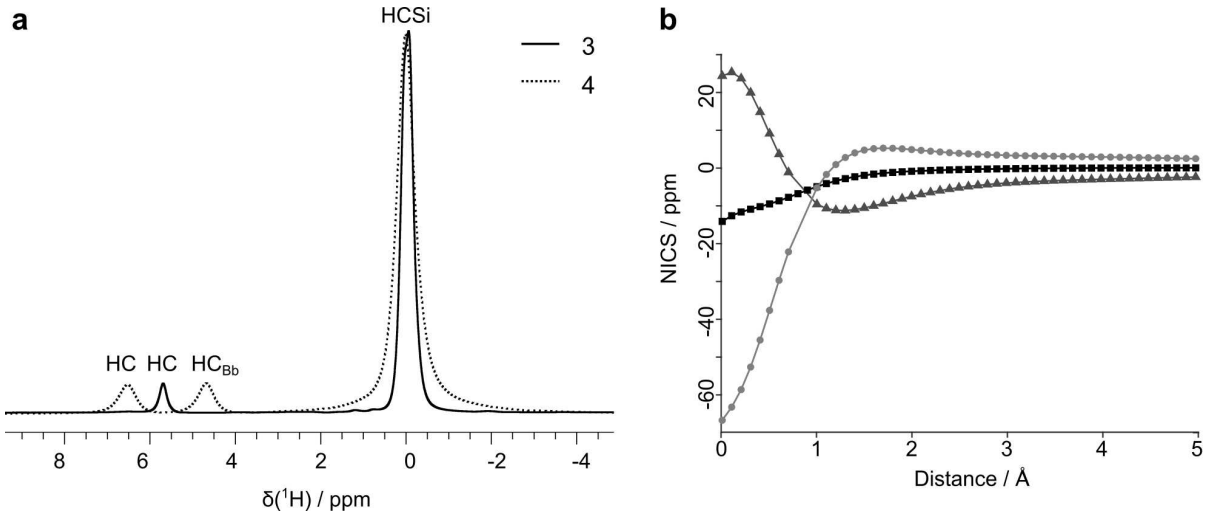

Figure 5. *Aromaticity probed by NICS calculations and proton-detected fast MAS experiments.* **a** ^{1}H spectrum of compounds **3** and **4** recorded at 16.4 T and 60 kHz MAS applying a Hahn echo sequence. The spectrum of **3** has been already reported by us in reference[38]. Assignment in accordance with solution-state NMR spectroscopic data.[4e,8] **b** NICS-scan (B3-LYP/def2-TZVP) curve of compound **3**. • – isotropic NICS value, ▲ – out-of-plane (σ_{zz}) NICS value, ● – in-plane ($\sigma_{xx}+\sigma_{yy}$) NICS value. For the distances of 0.8, 0.9 Å only the isotropic NICS value is shown as the calculated chemical-shift tensor (CST) contained imaginary eigenvalues.

follows what is considered characteristic for a 6π electron system.[23f] These results are highly similar to NICS calculations for group 14 pyramidanes (Scheme 1a, A=Ge, Sn, Pb) and the first reported borapyramidane (Scheme 1a, A=BCl) and support a picture of charge transfer from B_a to the pyramid base accompanied by a high degree of electron delocalization.[4f,6] Based on these findings, part of the extraordinarily strong shielding seen for the apical boron nuclei can be attributed to the shielding effect caused by the aromatic ring currents (see for example the ^{1}H resonances of water in a water-benzene complex[36]). Furthermore, the delocalized electron density resulting from the proposed three-dimensional aromaticity, as it was investigated for group 14 pyramidanes in reference[6] and reference[37], could further contribute to the electronic shielding effect and might explain as well why the proton resonances within the C_4- and C_4B-plane, are less deshielded than expected. For a more detailed analysis of the ^{11}B nuclear shielding using NBO and NCS analysis see the Supplementary Materials Section (Figures S10 and S11, Tables S4 and S5).

AIM calculations show that apex-base bonds possess both covalent and ionic contributions and support a charge transfer hypothesis

Bond topological analysis based on the AIM method was performed on borapyramidane **3** as a representative example to quantify the interatomic interactions from the C_4 pyramid base to the apical boron atom B_a.[24] The analysis revealed the presence of three bonding paths from the C_4-plane to the apical boron B_a, with no bond critical point obtained for the C_H–B_a path. Noteworthy, the C_H–B_a bond is the only bond in **3** for which a negative isotropic coupling constant was calculated and the electron density on the C_H atom is smaller than on the other carbon atoms of the pyramid plane (see Table S6). Analysis of the electron density ρ(r) and the Laplacian of the electron density $\nabla^2\rho$(r) allowed to further characterize the intramolecular interactions (see Table 3). While the electron density ρ(r) of the C_4-B_a bonds is not too different from that of other covalent interactions in the molecule, like B_b-C_{Bb}, the absolute value of the Laplacian $\nabla^2\rho$(r) is at least one order of magnitude smaller. This is in line with the experimentally determined ^{13}C-^{11}B isotropic coupling constants, which are around ^1J = 75–84 Hz for a typical 2c–2e boron-carbon bond, and at least one order of magnitude smaller for the boron-(apical)-carbon(basal) bonds. Based on the sign of the Laplacian, two C_4-B_a interactions are characterized as covalent and one as ionic. These findings are also reflected in the NBO calculations, where lower bond orders were found for the C_4-apex bonding (in **3** an average of 0.8).

The calculated group partial charges (Table 4) indicate an one-electron charge transfer from the B_a-iC_6F_5 unit to the C_4 base leading to an approximately single positive partial charge for B_a-iC_6F_5 and an approximately single negative partial charge for the base. This is in agreement with calculations for instance performed recently on sila[4]pyramidanes.[4a] The combined data supports a structural model as drawn in Scheme 3. This structural model coincides with the ring-current effects and electron delocalization contributing to the apical boron shielding discussed above.

Conclusions

We employed solid-state NMR spectroscopy supplemented with quantum-chemical calculations to investigate the solid-state bonding properties of of borapyramidanes with C_4 and C_4B bases, respectively.. ^{11}B MAS experiments reveal unusually low-

Table 3. AIM bond topological analysis of bora[4]pyramidane **3**. Displayed are the electron density (ρ(r)) and the electron density Laplacian ($\nabla^2\rho(r)$) for the obtained bond critical points (bcp) together with the corresponding bond types. Calculations were performed at a B3-LYP/def2-TZVP level-of-theory. [a] No bcp was determined. [b] Average of the four C–C bonds in the pyramid plane.

	ρ(r)	$\nabla^2\rho$(r)	Bond type based on ρ(r), $\nabla^2\rho$(r)
B_a-C_H	_[a]	_[a]	_[a]
B_a–C_{Si1}	0.143	−0.004	covalent
B_a–C_{Si2}	0.137	−0.015	covalent
B_a–C_{Bb}	0.143	0.065	ionic
B_a–iC_6F_5	0.185	−0.113	covalent
B_b–C_{Bb}	0.202	−0.139	covalent
C_4[b]	0.258	−0.566	covalent

Table 4. Group partial charges (*Q*(AIM)) for selected atom groups in compound **3**. Calculations were performed at a B3-LYP/def2-TZVP level of theory with the software AIMAll.

	Q(AIM)/e
[B_a(iC_6F_5)]	0.99
[C_4H]	−3.11
[$SiMe_3$][a]	0.77
[B_b(iC_6F_5)$_2$]	0.59

[a] Average of both TMS groups.

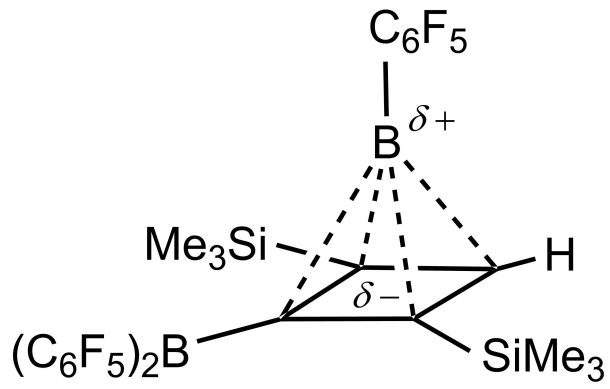

Scheme 3. Hypothetic bonding scenario proposed based on results from solid-state NMR and quantum-chemical calculations in bora[4]pyramidane **3**. The charges represent the group partial charges.

frequency shifted apical boron atoms in such compounds. Supported by NICS calculations, a contribution to the observed shielding is assigned to ring-current effects originating from the three-dimensional aromatic character in the pyramid base. The apical boron nucleus is described by rather small quadrupolar coupling constants of less than 0.9 MHz, indicating a small EFG around this atom, with the largest tensor component pointing towards the pyramid base. This is in contrast to the boron nuclei of the basal $-B(C_6F_5)_2$ substituents, which display quadrupolar coupling constants and asymmetry parameters typical for three-coordinated boron species (C_Q above 4 MHz and η_Q of 0.2). The slow quadrupolar relaxation in the solid state allowed determining isotropic ^{13}C-^{11}B coupling constants, ^1J, from the ^{13}C CP-MAS spectra serving as a criterion for bond covalence. For classical 2c–2e boron-carbon bonds, such as the one between the $-B(C_6F_5)_2$ substituents and the carbon of the C_4-plane, *J*-values on the order of 75–84 Hz were observed. In contrast, those for the boron(apical)-carbon(basal) bonds are at least one order of magnitude smaller. These findings are complemented with AIM bond topological analyses, which labels the boron(apical)-carbon(basal) bonds as polar covalent and indicates a charge transfer within the molecule leading to a positive partial charge at the apical boron atom and a negative partial charge delocalized over the base and the substituents. Combining the spectroscopic and quantum-chemical data, our data point to a bonding scenario in the studied borapyramidanes that can be best described as covalent with a high degree of polarity.

Experimental Section

Synthesis and general characterization of the investigated compounds **1**–**3** has been reported.[4e] The synthesis of compound **4** is briefly summarized in the Supplementary Information.[8]

Solid-state NMR

Solid-state NMR measurements were performed on wide-bore Bruker 500 MHz (11.7 T) and 700 MHz (16.4 T) spectrometers. The spectra were processed with the software Topspin (3.6.4 and 4.1.3, Bruker Biospin).

^{11}B spectra were measured on the 700 MHz spectrometer (^{11}B Larmor frequency of 224.7 MHz), with the exception of **1**, for which ^{11}B MAS EASY spectra were recorded on the 500 MHz spectrometer (^{11}B Larmor frequency of 160.5 MHz) as well. The spectra were recorded with Bruker 3.2 mm triple- or double-resonance probes at 20.0 kHz MAS and a sample temperature of around 283 K. To obtain ^{11}B MAS spectra in which line-shape interpretation is feasible, the spectral background originating from boron nitride in the solid-state NMR probes had to be eliminated. This was achieved by applying an EASY background suppression scheme.[39] Pulse parameters were optimized on the measured sample and signals were acquired following excitation with 90°–108° pulses of about 2.3–3.2 μs in length and repetition times of 60 s. The acquisition time was set to 11 ms. C_Q and η_Q parameters were extracted by line-shape fitting analysis using the DMFit software[40] (version #20190125), applying the *Q MAS* $^1/_2$ function. ^{11}B SATRAS[26] spectra were obtained by applying short pulses of flip angle 15°–50°, 0.7–2.3 μs in length with a repetition time of 60 s. The spectral width was increased, to approximately 5600 ppm, at an acquisition time of 5.7 ms. C_Q and η_Q parameters were extracted by line-shape fitting analysis using DMFit, applying the *Quad 1st* function. Chemical-shift calibration was achieved with a $NaBF_4$ standard.

^1H–^{13}C CP MAS spectra were measured on the 700 MHz spectrometer (^{13}C Larmor frequency of 176.1 MHz), with the exception of **4**, for which ^1H–^{13}C CP MAS spectra were recorded on both, the above and on the 500 MHz spectrometer (^{13}C Larmor frequency of 125.7 MHz). The spectra were recorded with Bruker 3.2 mm triple- or double-resonance probes at 17.0 kHz MAS and a sample temperature of around 283 K. Pulse parameters were optimized on the measured sample. ^1H 90° pulse lengths of 2.5 μs, a contact time of 1.5–3.5 ms and relaxation delays of 20–40 s were applied. Adiabatic CP transfer under the Hartmann-Hahn condition was achieved by a ramped-amplitude CP pulse,[41] with $\nu_{RF}(^1H)$ swept from 48 to 72 kHz. All spectra were acquired under SPINAL-64[42] proton decoupling, pulse length of 5.56 μs, during data acquisition. Multiplet structures were evaluated by line-shape fitting analysis using DMFit, applying the *Jmultiplet* function. Chemical-shift calibration was achieved with an adamantane standard relative to TMS.

^{29}Si MAS spectra were measured on the 700 MHz spectrometer (^{29}Si Larmor frequency of 139.1 MHz) with a Bruker 3.2 mm triple- or double-resonance probe at 17.0 kHz MAS and sample temperature of around 283 K. ^{29}Si MAS-NMR spectra were acquired applying a 90° hard pulse of 5 μs length and a relaxation delay of 80 s. ^1H-^{29}Si CP MAS spectra were acquired using a ^1H 90° pulse length of 2.5 μs, a contact time of 5 ms, and relaxation delays of 30 s were applied. Adiabatic CP transfer under the Hartmann-Hahn condition was achieved by a ramped-amplitude CP pulse[41], with $\nu_{RF}(^1H)$ swept from 48 to 72 kHz. The CP spectra were acquired under SPINAL-64[42] proton decoupling, pulse length of 5.56 μs, during data acquisition. Chemical-shift calibration was achieved with an octakis(trimethylsiloxy)silsesquioxane standard.

^1H-^{29}Si HETCOR spectra were measured on the 700 MHz spectrometer (^{29}Si Larmor frequency of 139.1 MHz) with a Bruker 3.2 mm double-resonance probe at 17.0 kHz MAS and a sample temperature of around 283 K. ^1H 90° pulse lengths of 2.5 μs, a contact time of 5 ms and relaxation delays of 15 s were applied. Adiabatic CP transfer under the Hartmann-Hahn condition was achieved by a ramped-amplitude CP pulse[41], with $\nu_{RF}(^1H)$ swept from 48 to 72 kHz. Four multiples of homonuclear frequency-switched Lee-Goldburg (FSLG)[43] decoupling with amplitude $\nu_1(^1H) = 100$ kHz were applied preceding the heteronuclear transfer and SPINAL-64 proton decoupling, pulse length of 5.56 μs, during data acquisition. Chemical-shift calibration was achieved with an octakis(trimethylsiloxy)silsesquioxane standard.

^1H MAS Hahn echo spectra were measured on the 700 MHz spectrometer with a Bruker 1.3 mm double-resonance probe at 60.0 kHz MAS and a sample temperature of around 283 K. ^1H 90° pulse lengths of 2.5 μs were used and relaxation delays of 15 s were applied. Chemical-shift calibration was achieved with an adamantane standard.

Ab initio calculations

All calculations were carried out using the program packages TURBOMOLE (version 7.3.0)[44] and GAUSSIAN (version GAUSSIAN09)[45]. Geometry optimizations were based on the provided crystal structures,[4e,8] with fixed heavy atom positions and were performed with the TURBOMOLE program on a DFT meta-GGA (TPSS[46]) level of theory, applying the D3 dispersion correction[47] and def2-TZVP[48] basis set. For all TURBOMOLE SCF calculations, an energy convergence criterion of 10^{-7} E_h was chosen

and for corresponding geometry optimization, the energy convergence criterion was set to $5x10^{-7}$ E_h. The integration grid was set to m4[49] and the RI approximation[50] was used.

The calculations of the nuclear electric quadrupole coupling tensors[22a,51] were based on the optimized geometries. Calculations of the electric field gradients were performed on a DFT GGA level of theory (B97-D[52]) using the program GAUSSIAN09. Analogous as in reference[17], the def2-TZVP basis set obtained from the EMSL database[53] was modified to include tighter basis functions (from the cc-pCVTZ basis set[54]) on the boron atom for a more accurate description of the region close to the boron nucleus. The GAUSSIAN output files were analyzed using the program EFGShield[22b], version 2.4, to determine C_Q and η_Q values. To visualize the EFG tensor, the DIAMOND software (version 4.6.8)[55] was used.

Magnetic-shielding calculations were performed with the GIAO (gauge-independent atomic orbitals) framework.[51,56] Shieldings were calculated on the B3-LYP[57] level of theory with the def2-TZVP[48] basis set using the TURBOMOLE program package. Chemical shifts are referenced to $BF_3{\cdot}Et_2O$ by using B_2H_6 ($\delta(B_2H_6) = 16.6$ ppm vs $BF_3{\cdot}Et_2O$) as an external standard ($\sigma^{B3-LYP}(B_2H_6) = 84.18$ ppm).[58]

NICS[23a–d] calculations were done in analogy to the magnetic shielding calculations by placement of ghost atoms without basis in the crystal structure. Ghost atoms were placed below the pyramid base on the axis apical boron – non mass-weighted ring centroid in distances of 0 to 5 Å (steps of 0.1 Å) to the ring centroid. Analogous to previous studies on group-14 pyramidanes,[6] obtained chemical-shift tensors were evaluated according to Stanger in terms of the in-plane component ($\sigma_{xx}+\sigma_{yy}$) and the out of plane component (σ_{zz}).[23e,f]

^{13}C-^{11}B indirect spin-spin coupling constants were calculated on a B3-LYP level of theory with the TZVP[59] basis set using the program GAUSSIAN09. The calculations were performed with the previously optimized molecular geometries.

The calculations of the natural bond orbitals (NBO)[25a–d] and natural localized molecular orbitals (NLMO)[25d] were based on the optimized geometries. Calculations of the NBO and NLMO were performed on a B3-LYP level of theory with the TZVP basis set using the program NBO3.1[60] integrated in GAUSSIAN09. The NBO output was visualized with the software GaussView.[61]

Natural chemical shift analysis (NCS)[62] was calculated based on the optimized geometries. Calculations were performed on a B3-LYP level of theory with the TZVP basis set using the program NBO3.1[60] integrated in GAUSSIAN09.

The analysis of the charge density according to the AIM method,[24] of **3** was performed in AIMAll[63] (version 19.10.12). The crystal structure was re-optimized as described above, including the heavy nuclei. The bond topology analysis was performed on the B3-LYP level of theory with the def2-TZVP basis set. Partial atomic charges were obtained by integration of the electron density.

Supporting Information

Additional references cited within the Supporting Information.[64–67]

Author Contributions

D.L. and N.T. performed the solid-state NMR experiments. D.L. performed NICS, NBO and NCS calculations and computed the NMR observables. Q.S. prepared the samples. C.M.L. performed the AIM analysis. D.L., N.T., H.E., G.K., C.M.L., G.E. and T.W. analysed and interpreted the data. D.L. wrote the initial draft, which has been edited by all authors. T.W. designed and supervised the study.

Acknowledgements

T.W. acknowledges support from the Deutsche Forschungsgemeinschaft (DFG, German Research Foundation, project number 455240421 and Heisenberg fellowship, project number 455238107) and the Max Planck Society. T.W. appreciates the funding by the Deutsche Forschungsgemeinschaft (DFG, German Research Foundation) under Germany's Excellence Strategy – Exzellenzcluster 2186 "The Fuel Science Center". We thank Dr. Baran Uluca-Yazgi (Max Planck Institute for Chemical Energy Conversion, Germany) for recording the ^{13}C spectrum of compound **4** at 11.7 T. Simulations done by D.L. were performed with computing resources granted by RWTH Aachen University under project thes1345. The research stay of D.L. at RWTH Aachen University was supported by a short-term research exchange grant from the IDEA League. D.L. and T.W. thank Prof. Dr. Matthias Ernst (ETH Zürich, Switzerland) for fruitful discussions. Open Access funding enabled and organized by Projekt DEAL.

Conflict of Interests

The authors declare no conflict of interest.

Data Availability Statement

The data that support the findings of this study are available from the corresponding author upon reasonable request.

Keywords: borapyramidane · chemical bonding · covalency · DFT · solid-state NMR

[1] a) V. Minkin, R. Minyaev, I. Zakharov, V. Avdeev, *Zh. Org. Khim.* **1978**, *14*, 3–15; b) V. I. Minkin, R. M. Minyaev, G. V. Orlova, *J. Mol. Struct.* **1984**, *110*, 241–253.
[2] a) V. I. Minkin, R. M. Minyaev, R. Hoffmann, *Russ. Chem. Rev.* **2002**, *71*, 869–892; b) V. I. Minkin, *Russ. Chem. Bull.* **2012**, *61*, 1265–1290; c) E. G. Lewars, *Modeling Marvels (Computational Anticipation of Novel Molecules)*, Springer, Berlin, **2008**.
[3] a) Q. Sun, C. Mück-Lichtenfeld, G. Kehr, G. Erker, *Nat. Chem. Rev.* **2023**, *7*, 732–746; b) V. Y. Lee, O. A. Gapurenko, *Chem. Commun.* **2023**, *59*, 10067–10086.
[4] a) T. Imagawa, L. Giarrana, D. M. Andrada, B. Morgenstern, M. Nakamoto, D. Scheschkewitz, *J. Am. Chem. Soc.* **2023**, *145*, 4757–4764; b) V. Y. Lee, O. A. Gapurenko, Y. Ito, T. Meguro, H. Sugasawa, A. Sekiguchi, R. M. Minyaev, V. I. Minkin, R. H. Herber, H. Gornitzka, *Organometallics* **2016**,

35, 346–356; c) A. Sekiguchi, T. Matsuo, H. Watanabe, *J. Am. Chem. Soc.* **2000**, *122*, 5652–5653; d) K. Takanashi, A. Inatomi, V. Y. Lee, M. Nakamoto, M. Ichinohe, A. Sekiguchi, *Eur. J. Inorg. Chem.* **2008**, 1752–1755; e) Q. Sun, C. G. Daniliuc, X. Yu, C. Mück-Lichtenfeld, G. Kehr, G. Erker, *J. Am. Chem. Soc.* **2022**, *144*, 7815–7821; f) V. Y. Lee, H. Sugasawa, O. A. Gapurenko, R. M. Minyaev, V. I. Minkin, H. Gornitzka, A. Sekiguchi, *J. Am. Chem. Soc.* **2018**, *140*, 6053–6056; g) V. Y. Lee, Y. Ito, A. Sekiguchi, H. Gornitzka, O. A. Gapurenko, V. I. Minkin, R. M. Minyaev, *J. Am. Chem. Soc.* **2013**, *135*, 8794–8797.

[5] a) V. I. Minkin, R. M. Minyaev, *Dokl. Chem.* **2002**, *385*, 203–206; b) E. Lewars, *J. Mol. Struct.* **1998**, *423*, 173–188; c) J. P. Kenny, K. M. Krueger, J. C. Rienstra-Kiracofe, H. F. Schaefer, *J. Phys. Chem. A* **2001**, *105*, 7745–7750; d) E. Lewars, *J. Mol. Struc.-Theochem* **2000**, *507*, 165–184.

[6] L. A. Leites, R. R. Aysin, S. S. Bukalov, V. Y. Lee, H. Sugasawa, A. Sekiguchi, *J. Mol. Struct.* **2017**, *1130*, 775–780.

[7] V. Y. Lee, H. Sugasawa, O. A. Gapurenko, R. M. Minyaev, V. I. Minkin, H. Gornitzka, A. Sekiguchi, *Chem. Eur. J.* **2016**, *22*, 17585–17589.

[8] Q. Sun, C. G. Daniliuc, C. Mück-Lichtenfeld, G. Kehr, G. Erker, manuscript submitted.

[9] a) T. Wiegand, H. Eckert, S. Grimme, in *Frustrated Lewis Pairs I: Uncovering and Understanding* (Eds.: G. Erker, D. W. Stephan), Springer Berlin Heidelberg, Berlin, Heidelberg, **2013**, pp. 291–345; b) R. Knitsch, M. Brinkkotter, T. Wiegand, G. Kehr, G. Erker, M. R. Hansen, H. Eckert, *Molecules* **2020**, *25*, 1400.

[10] B. Wrackmeyer, *Z. f. Naturforsch. B* **2015**, *70*, 421–424.

[11] S. E. Ashbrook, M. J. Duer, *Conc. Magn. Reson. A* **2006**, *28a*, 183–248.

[12] K. L. Moran, T. E. Gier, W. T. A. Harrison, G. D. Stucky, H. Eckert, K. Eichele, R. E. Wasylishen, *J. Am. Chem. Soc.* **1993**, *115*, 10553–10558.

[13] E. Lindner, R. Fawzi, H. A. Mayer, K. Eichele, K. Pohmer, *Inorg. Chem.* **1991**, *30*, 1102–1107.

[14] K. Eichele, R. E. Wasylishen, J. F. Corrigan, S. Doherty, A. J. Carty, Y. Sun, *Inorg. Chem.* **1993**, *32*, 121–123.

[15] a) G. Brunklaus, J. C. C. Chan, H. Eckert, S. Reiser, T. Nilges, A. Pfitzner, *Phys. Chem. Chem. Phys.* **2003**, *5*, 3768–3776; b) M. Scheer, L. Gregoriades, J. Bai, M. Sierka, G. Brunklaus, H. Eckert, *Chemistry* **2005**, *11*, 2163–2169; c) J. A. Tang, B. D. Ellis, T. H. Warren, J. V. Hanna, C. L. Macdonald, R. W. Schurko, *J. Am. Chem. Soc.* **2007**, *129*, 13049–13065.

[16] K. Eichele, R. E. Wasylishen, K. Maitra, J. H. Nelson, J. F. Britten, *Inorg. Chem.* **1997**, *36*, 3539–3544.

[17] T. Wiegand, H. Eckert, O. Ekkert, R. Fröhlich, G. Kehr, G. Erker, S. Grimme, *J. Am. Chem. Soc.* **2012**, *134*, 4236–4249.

[18] D. Massiot, F. Fayon, M. Deschamps, S. Cadars, P. Florian, V. Montouillout, N. Pellerin, J. Hiet, A. Rakhmatullin, C. Bessada, *Compt. Rend. Chim.* **2010**, *13*, 117–129.

[19] S. P. Brown, M. Perez-Torralba, D. Sanz, R. M. Claramunt, L. Emsley, *J. Am. Chem. Soc.* **2002**, *124*, 1152–1153.

[20] T. Wiegand, H. Eckert, J. Ren, G. Brunklaus, R. Fröhlich, C. G. Daniliuc, G. Lübbe, K. Bussmann, G. Kehr, G. Erker, S. Grimme, *J. Phys. Chem. A* **2014**, *118*, 2316–2331.

[21] a) D. B. Ravnsbaek, Y. Filinchuk, R. Cerny, M. B. Ley, D. Haase, H. J. Jakobsen, J. Skibsted, T. R. Jensen, *Inorg. Chem.* **2010**, *49*, 3801–3809; b) R. W. Schurko, I. Hung, S. Schauff, C. L. B. Macdonald, A. H. Cowley, *J. Phys. Chem. A* **2002**, *106*, 10096–10107; c) L. M. Arnbjerg, D. B. Ravnsbaek, Y. Filinchuk, R. T. Vang, Y. Cerenius, F. Besenbacher, J. E. Jorgensen, H. J. Jakobsen, T. R. Jensen, *Chem. Mater.* **2009**, *21*, 5772–5782.

[22] a) J. Autschbach, S. Zheng, R. W. Schurko, *Conepts Magn. Reson. A* **2010**, *36 A*, 84–126; b) S. Adiga, D. Aebi, D. L. Bryce, *Can. J. Chem.* **2007**, *85*, 496–505.

[23] a) Z. Chen, C. S. Wannere, C. Corminboeuf, R. Puchta, P. Schleyer, *Chem. Rev.* **2005**, *105*, 3842–3888; b) P. V. R. Schleyer, C. Maerker, A. Dransfeld, H. Jiao, N. J. R. van Eikema Hommes, *J. Am. Chem. Soc.* **1996**, *118*, 6317–6318; c) P. V. Schleyer, H. J. Jiao, N. J. R. V. Hommes, V. G. Malkin, O. L. Malkina, *J. Am. Chem. Soc.* **1997**, *119*, 12669–12670; d) P. V. R. Schleyer, M. Manoharan, Z. X. Wang, B. Kiran, H. Jiao, R. Puchta, N. J. R. van Eikema Hommes, *Org. Lett.* **2001**, *3*, 2465–2468; e) A. Stanger, *J. Org. Chem.* **2006**, *71*, 883–893; f) A. Stanger, *J. Org. Chem.* **2010**, *75*, 2281–2288.

[24] a) R. F. W. Bader, *Atoms in Molecules: A Quantum Theory*, Oxford University Press, Oxford, UK, **1990**; b) R. F. W. Bader, *J. Phys. Chem. A* **1998**, *102*, 7314–7323.

[25] a) J. P. Foster, F. Weinhold, *J. Am. Chem. Soc.* **1980**, *102*, 7211–7218; b) A. E. Reed, L. A. Curtiss, F. Weinhold, *Chem. Rev.* **1988**, *88*, 899–926; c) A. E. Reed, F. Weinhold, *J. Chem. Phys.* **1985**, *83*, 1736–1740; d) A. E. Reed, R. B. Weinstock, F. Weinhold, *J. Chem. Phys.* **1985**, *83*, 735–746; e) A. E. Reed, F. Weinhold, *J. Chem. Phys.* **1983**, *78*, 4066–4073.

[26] C. Jäger, W. Müller-Warmuth, C. Mundus, L. van Wüllen, *J. Non-Cryst. Solids* **1992**, *149*, 209–217.

[27] J. W. Weiss, D. L. Bryce, *J. Phys. Chem. A* **2010**, *114*, 5119–5131.

[28] D. L. Bryce, R. E. Wasylishen, M. Gee, *J. Phys. Chem. A* **2001**, *105*, 3633–3640.

[29] R. K. Harris, J. Bowles, I. R. Stephenson, E. H. Wong, *Spectrochim. Acta* **1988**, *44*, 273–276.

[30] T. Matsuo, A. Sekiguchi, *Bull. Chem. Soc. Jpn.* **2004**, *77*, 211–226.

[31] B. Wrackmeyer, *Prog. Nucl. Magn. Reson. Spectrosc.* **1979**, *12*, 227–259.

[32] R. K. Harris, A. C. Olivieri, *Prog. Nucl. Magn. Reson. Spectrosc.* **1992**, *24*, 435–456.

[33] S.-W. Oh, J. W. E. Weiss, P. A. Kerneghan, I. Korobkov, K. E. Maly, D. L. Bryce, *Magn. Reson. Chem.* **2012**, *50*, 388–401.

[34] H.-O. Berger, H. Nöth, B. Wrackmeyer, *Chem. Ber.* **1979**, *112*, 2884–2893.

[35] S. N. Steinmann, D. F. Jana, J. I.-C. Wu, P. v. R. Schleyer, Y. Mo, C. Corminboeuf, *Angew. Chem. Int. Ed.* **2009**, *48*, 9828–9833.

[36] E. Bartalucci, A. A. Malär, A. Mehnert, J. B. Kleine Büning, L. Günzel, M. Icker, M. Borner, C. Wiebeler, B. H. Meier, S. Grimme, B. Kersting, T. Wiegand, *Angew. Chem. Int. Ed. Engl.* **2023**, *62*, e202217725.

[37] R. R. Aysin, S. S. Bukalov, *Mendeleev Commun.* **2021**, *31*, 481–483.

[38] E. Bartalucci, D. J. Luder, N. Terefenko, A. A. Malär, C. Bolm, M. Ernst, T. Wiegand, *Phys. Chem. Chem. Phys.* **2023**, *25*, 19501–19511.

[39] a) C. Jäger, F. Hemmann, *Solid State Nucl. Magn. Reson.* **2014**, *57–58*, 22–28; b) C. Jäger, F. Hemmann, *Solid State Nucl. Magn. Reson.* **2014**, *63–64*, 13–19.

[40] D. Massiot, F. Fayon, M. Capron, I. King, S. Le Calve, B. Alonso, J. O. Durand, B. Bujoli, Z. H. Gan, G. Hoatson, *Magn. Reson. Chem.* **2002**, *40*, 70–76.

[41] a) S. Hediger, B. H. Meier, R. R. Ernst, *Chem. Phys. Lett.* **1995**, *240*, 449–456; b) S. Hediger, B. H. Meier, N. D. Kurur, G. Bodenhausen, R. R. Ernst, *Chem. Phys. Lett.* **1994**, *223*, 283–288.

[42] B. M. Fung, A. K. Khitrin, K. Ermolaev, *J. Magn. Reson.* **2000**, *142*, 97–101.

[43] a) A. Bielecki, A. C. Kolbert, H. J. M. De Groot, R. G. Griffin, M. H. Levitt, *Adv. Magn. Reson.* **1990**, *14*, 111–124; b) M. H. Levitt, A. C. Kolbert, A. Bielecki, D. J. Ruben, *Solid State Nucl. Magn. Reson.* **1993**, *2*, 151–163; c) M. Mehring, J. S. Waugh, *Phys. Rev. B* **1972**, *5*, 3459–3471.

[44] a) R. Ahlrichs, M. Bär, M. Häser, H. Horn, C. Kolmel, *Chem. Phys. Lett.* **1989**, *162*, 165–169.

[45] M. J. Frisch, G. W. Trucks, H. B. Schlegel, G. E. Scuseria, M. A. Robb, J. R. Cheeseman, G. Scalmani, V. Barone, B. Mennucci, G. A. Petersson, H. Nakatsuji, M. Caricato, X. Li, H. P. Hratchian, A. F. Izmaylov, J. Bloino, G. Zheng, J. L. Sonnenberg, M. Hada, M. Ehara, K. Toyota, R. Fukuda, J. Hasegawa, M. Ishida, T. Nakajima, Y. Honda, O. Kitao, H. Nakai, T. Vreven, J. A. Montgomery, Jr., J. E. Peralta, F. Ogliaro, M. Bearpark, J. J. Heyd, E. Brothers, K. N. Kudin, V. N. Staroverov, R. Kobayashi, J. Normand, K. Raghavachari, A. Rendell, J. C. Burant, S. S. Iyengar, J. Tomasi, M. Cossi, N. Rega, J. M. Millam, M. Klene, J. E. Knox, J. B. Cross, V. Bakken, C. Adamo, J. Jaramillo, R. Gomperts, R. E. Stratmann, O. Yazyev, A. J. Austin, R. Cammi, C. Pomelli, J. W. Ochterski, R. L. Martin, K. Morokuma, V. G. Zakrzewski, G. A. Voth, P. Salvador, J. J. Dannenberg, S. Dapprich, A. D. Daniels, Ö. Farkas, J. B. Foresman, J. V. Ortiz, J. Cioslowski, D. J. Fox, *Gaussian 09*, Gaussian, Inc., Wallingford CT, **2009**.

[46] J. Tao, J. P. Perdew, V. N. Staroverov, G. E. Scuseria, *Phys. Rev. Lett.* **2003**, *91*, 146401.

[47] S. Grimme, J. Antony, S. Ehrlich, H. Krieg, *J. Chem. Phys.* **2010**, *132*, 154104.

[48] F. Weigend, R. Ahlrichs, *Phys. Chem. Chem. Phys.* **2005**, *7*, 3297–3305.

[49] O. Treutler, R. Ahlrichs, *J. Chem. Phys.* **1995**, *102*, 346–354.

[50] a) K. Eichkorn, F. Weigend, O. Treutler, R. Ahlrichs, *Theor. Chem. Acc.* **1997**, *97*, 119–124; b) K. Eichkorn, O. Treutler, H. Öhm, M. Häser, R. Ahlrichs, *Chem. Phys. Lett.* **1995**, *240*, 283–290.

[51] M. Kaupp, M. Bühl, V. G. Malkin, *Calculation of NMR and EPR parameters*, Wiley-VCH, **2004**.

[52] S. Grimme, *J. Comput. Chem.* **2006**, *27*, 1787–1799.

[53] a) D. Feller, *J. Comput. Chem.* **1996**, *17*, 1571–1586; b) K. L. Schuchardt, B. T. Didier, T. Elsethagen, L. Sun, V. Gurumoorthi, J. Chase, J. Li, T. L. Windus, *J. Chem. Inf. Model.* **2007**, *47*, 1045–1052.

[54] a) D. E. Woon, T. H. Dunning, *J. Chem. Phys.* **1995**, *103*, 4572–4585; b) K. A. Peterson, T. H. Dunning, *J. Chem. Phys.* **2002**, *117*, 10548–10560.

[55] Diamond - Crystal and Molecular Structure Visualization, Crystal Impact - Dr. H. Putz & Dr. K. Brandenburg GbR, Kreuzherrenstr. 102, 53227 Bonn, Germany, https://www.crystalimpact.de/diamond.

[56] R. Ditchfield, *Mol. Phys.* **1974**, *27*, 789–807.

[57] a) A. D. Becke, *J. Chem. Phys.* **1993**, *98*, 5648–5652; b) P. J. Stephens, F. J. Devlin, C. F. Chabalowski, M. J. Frisch, *J. Phys. Chem.* **1994**, *98*, 11623–11627.
[58] a) I. Antol, Z. Glasovac, M. Eckert-Maksić, *New J. Chem.* **2004**, *28*, 880–886; b) T. Onak, M. Diaz, M. Barfield, *J. Am. Chem. Soc.* **2002**, *117*, 1403–1410; c) M. Bühl, P. v. R. Schleyer, *J. Am. Chem. Soc.* **1992**, *114*, 477–491; d) T. Onak, H. Landesman, R. Williams, I. Shapiro, *J. Phys. Chem.* **1959**, *63*, 1533–1535.
[59] A. Schäfer, C. Huber, R. Ahlrichs, *J. Chem. Phys.* **1994**, *100*, 5829–5835.
[60] E. D. Glendenning, A. E. Reed, J. E. Carpenter, F. Weinhold, *NBO 3.1*.
[61] R. Dennington, T. A. Keith, J. M. Millam, *GaussView (version 6.0.16)*.
[62] J. A. Bohmann, F. Weinhold, T. C. Farrar, *J. Chem. Phys.* **1997**, *107*, 1173–1184.
[63] *AIMAll (Version 19.10.12), Todd A. Keith, TK Gristmill Software, Overland Park KS, USA, 2019 (aim.tkgristmill.com)*.
[64] S. Yruegas, K. Huang, D. J. D. Wilson, J. L. Dutton, C. D. Martin, *Dalton Trans.* **2016**, *45*, 9902–9911.
[65] Natick. MATLAB R2019b. Massachusetts: The MathWorks Inc.
[66] N. F. Ramsey, *Phys. Rev.* **1950**, *78*, 699–703.
[67] a) A. E. Alain, Y. Shoji, T. Fukushima, D. L. Bryce, *Inorg. Chem.* **2015**, *54*, 11889–11896; b) B. Zhou, V. K. Michaelis, Y. Yao, B. L. Sherriff, S. Kroeker, Y. Pan, *CrystEngComm* **2014**, *16*, 10418–10427.

Manuscript received: November 7, 2023
Accepted manuscript online: December 11, 2023
Version of record online: January 3, 2024